Helicopter noise footprint prediction in unsteady maneuvers

Gennaretti, Massimo; Bernardini, Giovanni; Serafini, Jacopo; Anobile, Alessandro; Hartjes, Sander

DOI
10.1177/1475472X17709927

Publication date
2017

Document Version
Final published version

Published in
International Journal of Aeroacoustics (online)

Article

aeroacoustics

International Journal of Aeroacoustics
2017, Vol. 16(3) 165–180

DOI: 10.1177/1475472X17709927
journals.sagepub.com/home/jae

SAGE

Helicopter noise footprint prediction in unsteady maneuvers

Massimo Gennaretti,[1] Giovanni Bernardini,[1] Jacopo Serafini,[1] Alessandro Anobile[2] and Sander Hartjes[3]

Abstract

This paper investigates different methodologies for the evaluation of the acoustic disturbance emitted by helicopter's main rotors during unsteady maneuvers. Nowadays, the simulation of noise emitted by helicopters is of great interest to designers, both for the assessment of the acoustic impact of helicopter flight on communities and for the identification of optimal-noise trajectories. Typically, the numerical predictions consist of the atmospheric propagation of a near-field noise model, extracted from an appropriate database determined through steady-state flight simulations/measurements (quasi-steady approach). In this work, three techniques for maneuvering helicopter noise predictions are compared: one considers a fully unsteady solution process, whereas the others are based on quasi-steady approaches. These methods are based on a three-step solution procedure: first, the main rotor aeroelastic response is evaluated by a nonlinear beam-like rotor blade model coupled with a boundary element method for potential flow aerodynamics; then, the aeroacoustic near field is evaluated through the 1A Farassat formulation; finally, the noise is propagated to the ground by a ray tracing model. Only the main rotor component is examined, although tail rotor contribution might be included as well. The numerical investigation examines the differences among the noise predictions provided by the three techniques, focusing on the assessment of the reliability of the results obtained through the two quasi-steady approaches as compared with those from the fully unsteady aeroacoustic solver.

Keywords

Unsteady aeroacoustics, helicopter, near and far field noise

Date received: 31 May 2016; accepted: 10 April 2017

[1]Department of Engineering, Roma Tre University, Rome, Italy
[2]Faculty of Engineering, The University of Nottingham, Nottingham, UK
[3]Aerospace Engineering, Delft University of Technology, Delft, the Netherlands

Corresponding author:
Massimo Gennaretti, Department of Engineering, Roma Tre University, Via della Vasca Navale 79, Rome 00146, Italy.
Email: m.gennaretti@uniroma3.it

Introduction

Nowadays, the prediction of noise generated aerodynamically by helicopters represents a crucial issue for rotorcraft researchers and designers. Indeed, the capability of evaluating the radiated sound in terms of magnitude and directivity pattern has a fundamental role in estimating acoustic impact and detectability of the noise source, as well as in developing strategies for reducing noise disturbances emitted by helicopter operations.

In the recent past, numerical tools suited to the determination of minimum-noise, optimal trajectories have been developed to alleviate the ground acoustic impact of helicopters (and, more generally, rotorcraft).[1–3] These tools usually combine a flight mechanics solver for trajectory simulation, a near-field noise radiation model (acoustic source), a far-field noise propagation model, and a geographic information system to let the optimization process consider orography and population density of the area of interest. In this framework, as near-field noise it is intended the noise radiated in proximity of the rotorcraft, i.e. at distances where atmospheric absorption, ground reflection, and wind effects are still negligible. It is affected by monopole and dipole propagation effects, differently from the far-field noise which is dominated by monopole-type radiation.

Considering arbitrary unsteady flight conditions (including turns, descent angle changes, accelerations, and decelerations), the noise source model has to be updated in accordance with the instantaneous flight condition experienced by the helicopter during the maneuver. In order to avoid numerically expensive predictions, this is usually accomplished by selecting the near-field model (provided in terms of sound spectrum distribution over a hemisphere rigidly connected to the helicopter—the so-called noise hemisphere) from an appropriate database related to rectilinear, steady-state flights, defined in a domain of parameters suitably characterizing the noise source state (quasi-steady acoustic approach).[1–4]

It is worth observing that a similar approach has been applied in the CleanSky project MANOEUVRES for developing a helicopter in-flight noise monitoring system (namely, the pilot acoustic indicator (PAI)), aimed at making the pilot aware of the produced acoustic impact, and thereby able to adequately react in case of excessive disturbance.[5] Indeed, the PAI relies on a noise real-time estimation algorithm that selects noise hemispheres from a database as functions of the current flight parameters.

However, unsteady effects arising during helicopter maneuvers may potentially strongly affect the emitted noise because of the corresponding inertial and aerodynamic loads variations, as well as pitch, roll, and yaw motion that, instead, may cause significant shifts in noise directivity.[6] Therefore, the selection of steady-state flight acoustic sources suitable for approximating noise radiated by a maneuvering helicopter is not a trivial issue. Usually, this is accomplished in terms of a set of flight parameters chosen to characterize the noise source state. The most common criteria adopted consider either advance ratio and flight-path slope angle (approach A, in the following), or advance ratio, rotor thrust coefficient, and rotor disk orientation with respect to relative wind (approach B, in the following).[1,2,4]

The aim of this work is the assessment of the accuracy of these criteria in estimating the acoustic disturbance generated by maneuvering helicopters, through correlations with predictions provided by a fully unsteady solver. The attention is focused on the main rotor, but tail rotor contribution might be similarly included.

The evaluation of noise radiated by maneuvering rotorcraft is not an easy task that has been addressed by a restricted number of researchers in the last decades.[6–9] It requires the extension of the commonly used steady flight solvers to nonperiodic blade motion and

loading, larger time scales of analysis, as well as the generalization of the numerical scheme applied to evaluate signal propagation. Taking into account these issues, here, the near-field aeroacoustic simulation is carried out by application of the retarded-time formulation 1A developed by Farassat,[10] as solution of the Ffowcs Williams and Hawkings equation.[11] Then, noise propagation through the atmosphere is predicted by a ray tracing model, which takes into account ground reflection and atmospheric effects (such as temperature gradient, relative humidity, wind speed, and direction).[3]

Given that blade–vortex interactions (BVIs) often represent an important source of noise in maneuvering flights (especially in ground approaches), the rotor blade pressure distribution is computed by a free-wake, aerodynamic/aeroelastic tool capable of capturing, with appropriate level of accuracy, wake vorticity, and wake-blade miss distance. In particular, main rotor loads and aeroelastic response are evaluated through a modal formulation applied to a nonlinear beam-like rotor blade model,[12,13] coupled with a three-dimensional, boundary element method (BEM) for the solution of free-wake, potential flows.[14] Steady aeroelastic solutions are obtained by a harmonic-balance approach,[15] whereas fully unsteady solutions are evaluated through a time-marching procedure based on the Newmark-β integration scheme.[16]

Methods for maneuver noise prediction

Noise emitted by helicopters during unsteady maneuvers is strongly affected by the flown trajectory features (namely, speed, flight-path slope angle, and radius of turns time evolutions). As mentioned above, typically, computational tools aimed at this kind of analyses consider noise hemispheres derived from databases of steady, straight-flight acoustic simulations. Such an approach is based on the assumption of simulating the near-field acoustic disturbance through a sequence of equivalent steady-flight predictions suitably associated to the evolving operating conditions.

In this work, the noise equivalence between steady and unsteady flight conditions is defined following two different approaches. In approach A, similarity of advance ratio, μ, and flight-path angle, γ, is assumed to guarantee the similarity of the emitted noise, whereas in approach B, μ, rotor thrust coefficient, C_T, and rotor disk orientation with respect to relative wind, α_{TPP}, are considered as the parameters that characterize noise equivalence between different flight maneuvers. This means that, for a given unsteady flight condition, in approach A the noise source is determined by extracting the noise hemisphere corresponding to the same values of μ and γ from the steady-flight database, whereas in approach B the noise source is determined as the one associated to the same values of μ, C_T, and α_{TPP} (see also Gennaretti et al.[16,17]).

In order to assess the quality of the acoustic predictions obtained by these approaches, their simulations are compared with those determined by the fully unsteady solution (approach C) based on the general aeroacoustic formulation described in ''Near-field noise prediction'' section. More specifically, the method of analysis consists of the following steps:

(i) for a given unsteady maneuver, time histories of the corresponding pilot commands and flight conditions are identified by a comprehensive helicopter aeromechanics solver;[17]

(ii) for selected points along the trajectory, trim commands and flight conditions corresponding to the steady, rectilinear flights defined by the parameters characterizing approach A and approach B are determined through the same aeromechanics solver;
(iii) a high-fidelity aerodynamic/aeroelastic solver (capable of capturing effects due to complex phenomena like BVIs, see Appendix 1) provides the pressure loads arising over the rotor blades throughout the unsteady maneuver (approach C), as well as during the steady flights of approaches A and B;
(iv) near-field noise sound pressure level (SPL) distributions corresponding to the three approaches are evaluated over a hemisphere rigidly connected to the helicopter;
(v) noise footprints on the ground are radiated from the acoustic hemispheres by approaches A, B, and C, and the corresponding results are compared.

The flight dynamics tool applied in steady flight trimming and unsteady maneuver identification applies a low-fidelity main rotor model suited for this kind of problems.[17] This fact combined with the observation that the prediction of rotor acoustic disturbance requires accurate evaluation of blade dynamics and aerodynamics (especially when BVI phenomena occur) motivates the introduction of high-fidelity aeroelastic and aerodynamic solvers in the third step of the presented analysis.

Aeroacoustic analysis of arbitrary unsteady maneuvers

The prediction of noise radiated by maneuvering rotorcraft is determined by a two-step approach, consisting of the near-field noise hemisphere evaluation (acoustic source), followed by the far-field propagation through atmosphere. The main feature of the noise hemispheres used as acoustic sources is that the sound propagation outside of them is of monopole type.

In the next subsections, the methodologies applied for near-field and far-field noise evaluation are outlined, providing in Appendix 1 a brief description of the aerodynamic/aeroelastic solver used to determine rotor blade data needed by the near-field acoustic formulation.

Near-field noise prediction

The noise emitted by rotor blades is evaluated through the widely used boundary integral formulation developed by Farassat[10] for the solution of the well-known Ffowcs Williams and Hawkings equation,[11] which governs the propagation of acoustic disturbances aerodynamically generated by moving bodies. When the rotor blades operate far from the transonic/supersonic regime, it yields the aeroacoustic field as a superposition of two terms: the thickness noise, p'_T, depending on blade geometry and kinematics

$$4\pi p'_T(\mathbf{x},t) = \int_{S_B}\left[\frac{\rho_0 \dot{v}_n}{r|1-M_r|^2}\right]_\tau \mathrm{d}S(\mathbf{y}) + \int_{S_B}\left[\frac{\rho_0 v_n\left(r\,\dot{\mathbf{M}}\cdot\hat{\mathbf{r}} + c_0 M_r - c_0 M^2\right)}{r^2|1-M_r|^3}\right]_\tau \mathrm{d}S(\mathbf{y}) \quad (1)$$

and the loading noise, p'_L, related to the distribution of pressure over blade surfaces

$$4\pi p'_L(\mathbf{x},t) = \frac{1}{c_0}\int_{S_B}\left[\frac{\dot{\tilde{p}}\mathbf{n}\cdot\hat{\mathbf{r}} + \tilde{p}\,\dot{\mathbf{n}}\cdot\hat{\mathbf{r}}}{r|1-M_r|^2}\right]_\tau \mathrm{d}S(\mathbf{y}) + \int_{S_B}\left[\frac{\tilde{p}\mathbf{n}\cdot\hat{\mathbf{r}} - \tilde{p}\mathbf{M}\cdot\mathbf{n}}{r^2|1-M_r|^2}\right]_\tau \mathrm{d}S(\mathbf{y})$$

$$+\frac{1}{c_0}\int_{S_B}\left[\frac{\tilde{p}\mathbf{n}\cdot\hat{\mathbf{r}}}{r^2|1-M_r|^3}r\dot{\mathbf{M}}\cdot\hat{\mathbf{r}}\right]_\tau \mathrm{d}S(\mathbf{y})+\int_{S_B}\left[\frac{\tilde{p}\mathbf{n}\cdot\hat{\mathbf{r}}}{r^2|1-M_r|^3}(M_r-M^2)\right]_\tau \mathrm{d}S(\mathbf{y}) \tag{2}$$

In the above equations, $\mathbf{r}$ denotes the distance between observer position, $\mathbf{x}$, and source position, $\mathbf{y}$, whereas $\hat{\mathbf{r}}=\mathbf{r}/r$ is the unit vector along the source–observer direction, with $r=||\mathbf{r}||$. In addition, c_0 and ρ_0 are the speed of sound and the density in the undisturbed medium, respectively, $\tilde{p}=(p-p_0)$ with p_0 representing the undisturbed medium pressure, $\mathbf{M}=\mathbf{v}_B/c_0$ with $\mathbf{v}_B$ denoting the body velocity, $M=||\mathbf{M}||$, $M_r=\mathbf{M}\cdot\hat{\mathbf{r}}$, and $v_n=\mathbf{v}_B\cdot\mathbf{n}$, where $\mathbf{n}$ is the outward blade surface unit normal vector. Further, $\dot{v}_n$, $\dot{\mathbf{n}}$, and $\dot{\mathbf{M}}$ denote time derivatives of v_n, $\mathbf{n}$, and $\mathbf{M}$, observed in a frame of reference fixed with the undisturbed medium.

The integrals appearing in equations (2) and (1) are evaluated by a zeroth-order BEM: the blade surface is divided into quadrilateral panels, and the integrand factors of kernels are assumed to be uniformly distributed within each panel, with values equal to those at the centroids. Notation $[\ldots]_\tau$ indicates that these quantities are evaluated at the delayed source time, $\tau=t-\theta$, where θ is the time taken by the signal started from $\mathbf{y}\in S_B$ to arrive at $\mathbf{x}$ at time t.[10]

Excluding applications in which transonic effect may arise because of high blade tip speed, in problems dealing with weakly loaded rotors, thickness and loading noise are of comparable magnitude (but different directivity), while for rotors that are strongly loaded and/or subject to impulsive load changes, thickness noise contribution tends to be negligible and the acoustic disturbance is dominated by loading noise. Rotors in BVI conditions fall within this category of acoustic phenomena.

Commonly, aeroacoustic formulations for helicopter rotor analysis consider steady, rectilinear, trimmed flights. In these operating conditions both kinematics and aerodynamics events are time periodic thus yielding time-periodic contributions to the aeroacoustic formulation. In contrast, during unsteady helicopter maneuvers, kinematic and aerodynamic terms are nonperiodic, thus increasing the complexity of the algorithms to be applied for implementing equations (2) and (1). In particular, they require the knowledge of the time histories of vehicle and blade kinematics, for a time interval length depending on observer location, as defined by time delays, θ, appearing in thickness and loading noise expressions, which are obtained as solutions of the following nonlinear equation

$$\left\|\mathbf{x}(t)-\mathbf{y}(t-\theta)\right\|=c_0\theta \tag{3}$$

Indeed, time histories of center of mass trajectory and velocity, vehicle attitude, and angular velocity are necessary data to evaluate instantaneous values of kernels and integral coefficients of the discretized versions of equations (2) and (1), as well as the boundary conditions of the aerodynamic formulation applied to determine the nonperiodic blade loads (see Appendix 1).

Far-field noise propagation

The propagation losses between source and receiver, and the resulting noise exposure on the ground are determined through a three-step process,[18] briefly outlined in the following (a more detailed description is given in Appendix 2).

First, the path of the sound ray between the helicopter and a ground-based receiver is determined. Rather than using an integration over time of the ray path, a geometrical

approach is used, where the atmosphere is represented as a number of layers with constant speed of sound gradients. Refraction is then accounted for within the layers rather than between the integration steps as in classical ray tracing approaches. This approach greatly reduces the number of integration steps due to the limited number of layers required, and as such allows the numerical determination of the ray paths between the source and a discrete number of receiver positions.

In the second step, the bearing between the source and the receiver and the launch angle of the sound ray at the source determines the azimuth and elevation angles where the ray passes through the hemisphere, hence providing the SPL emitted at the source. Since the ray tracing method described above is independent of the frequency, the source noise levels for all available frequencies can be determined concurrently.

With the source noise level and the ray path known, the propagation losses can be determined. The algorithm takes into account three attenuation effects: (i) atmospheric attenuation (or absorption) is accounted for using the method defined by International Civil Aviation Organization (ICAO)[19] and depends on the ray path and sound frequency; (ii) spreading loss is accounted for, which includes the effects of focusing in a refracting atmosphere[20]; (iii) the ground effect is included using the approach defined by Delaney and Bazley,[21] in order to account for secondary rays reflecting off different ground surface types. In addition to the three attenuation effects mentioned above, also the sound level in the shadow zone is determined. Based on the approach developed by Arntzen et al.,[22] the strong decrease of the sound level at the transition between the illuminated and the shadow zone is determined, as well as the noise levels penetrating the shadow zones due to ground waves, diffraction and scattering due to turbulence.

For each of the time steps available in the hemisphere samples, the total sound energy reaching the ground is determined based on the source noise levels and the propagation losses. This A-weighted sound level in each of the grid points can then be integrated over the execution time of the trajectory to obtain the sound exposure level of the full trajectory.

Numerical results

The numerical investigation on noise prediction capability of the approaches described in "Methods for maneuver noise prediction" section concerns a specific unsteady flight of a lightweight helicopter model inspired by the BO-105. It is a relatively small, multipurpose helicopter with an empty mass of about 1200 kg and a maximum gross mass of 2300 kg. It has a four-bladed, hingeless, counterclockwise rotating main rotor of 4.91 m radius, with blade precone angle of 2.5°. Inertial and elastic characteristics of the helicopter model used here are in Dang-Vu et al.[23]

The unsteady maneuver considered consists of an initial level, steady rectilinear flight, followed by a straight, decelerated descent, and a final pull up that precedes a steady level turn.[17] The time histories of the main flight parameters (namely, altitude, advance ratio, flight-path slope angle, thrust coefficient, and tip-path-plane angle of attack) determined by the aeromechanics solver for the flown trajectory are shown in Figure 1. In this figure, moreover, some noteworthy maneuver points are marked: these identify the flight conditions where the quasi-steady aeroacoustic approaches A and B are compared with the fully unsteady solution, approach C.

The first point corresponds to the flight time $t = 4$ s, and represents the beginning of the decelerated descent, following to a curved trajectory segment in the vertical plane

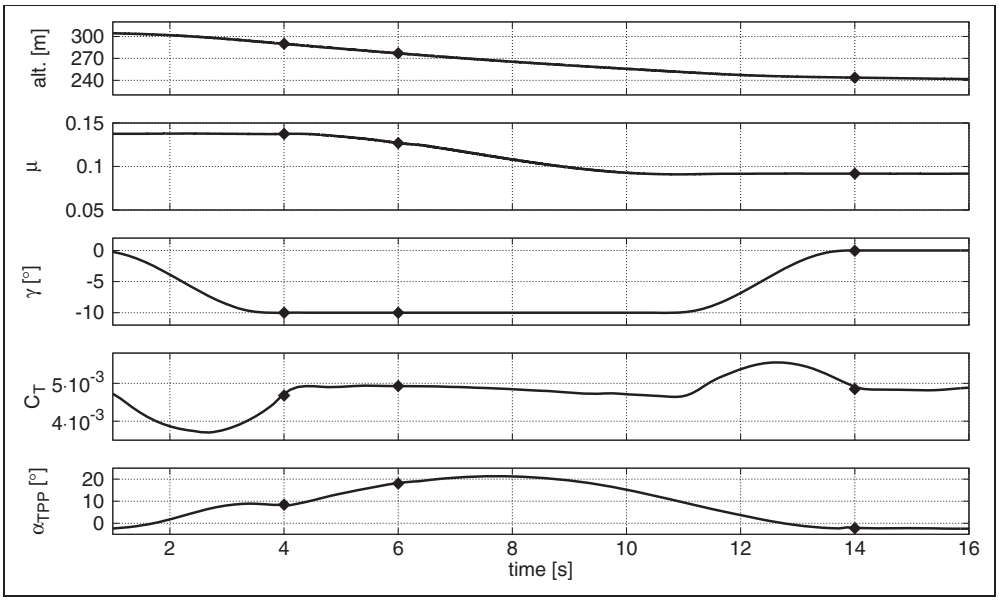

Figure 1. Evolution of flight parameters during the considered maneuver.

characterized by a remarkable variation of the thrust coefficient for $1 < t < 4$ s (see Figure 1). At $t = 6$ s (second mark) the helicopter is in the middle of the decelerated descent at constant flight-path angle, with the tip-path plane tilted rearward, as depicted in Figure 1. The last point of analysis is at $t = 14$ s, that corresponds to the end of the pull-up maneuver, performed to achieve the final level flight.

It is worth noting that the unsteady effects at point one and three greatly affect the load factor. Indeed, in both cases the helicopter experiences a transition between two different flight conditions with a significant variation of the thrust coefficient, C_T (see Figure 1). A different behavior can be observed at $t = 6$ s, when the helicopter is decelerating during a rectilinear descent flight, and the unsteady effects influence its attitude. Indeed, in such a condition the inertial loads act along the tangent to the trajectory, thus altering rotor attitude with respect to wind, namely α_{TPP} (these inertial effects are taken into account in approach B, but are hidden to approach A).

In the following, the comparisons among the acoustic predictions provided by the three aeroacoustic approaches are shown for the three points selected along the trajectory. The numerical results are presented both in terms of overall sound pressure level (OASPL) evaluated over hemispheres of radius $R = 150$ m centered at the main rotor hub and in terms of A-weighted SPLs (dB_A) determined on the ground surface underneath the flight path (the corresponding helicopter altitude is shown in Figure 1). In order to avoid the onset of leakage problems for the outcomes related with the fully unsteady simulations, the OASPL has been computed by applying a 3/rev-long Hanning window, centered at the trajectory point considered. Top views of the noise hemispheres are illustrated, along with the corresponding instantaneous noise footprints. Note that at $t = 0$ s the helicopter flies over the origin of the axes, whereas at $t = 15$ s it passes over the point of coordinates $x = 360$ m, $y = 0$ m (with x denoting flight direction).

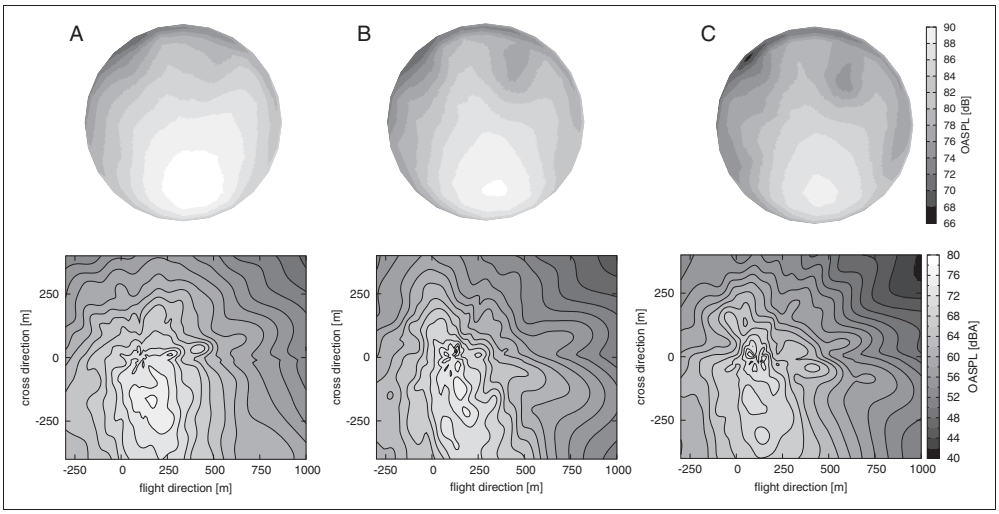

Figure 2. Noise hemispheres and noise footprints at $t = 4$ s.

First, the aeroacoustic predictions provided by approach A, approach B, and the fully unsteady aeroacoustic solver for $t = 4$ s are shown in Figure 2. As already mentioned, at this point the noise is significantly affected by the inertial effects due to trajectory curvature, strictly related to the remarkable variation of the thrust coefficient occurring at $1 < t < 4$ s. BVI effects are also present because of the beginning of the descent path.

The comparison of the results reveals that approach A, being unable to capture the disk loading alleviation due to unsteady maneuver, predicts significantly higher noise than that from approach C. Conversely, approach B provides levels of acoustic disturbance closer to those from the unsteady simulation. Focusing only on the highest noise level, an overestimation up to 3 dB is provided by approach A, whereas a maximum discrepancy of about 2 dB is observed in predictions by approach B. Noise effects related to BVI events seem to be captured by the three approaches, and noise directivity predicted on both the hemisphere and the ground is comparable.

The results for the flight condition occurring at $t = 6$ s are shown in Figure 3. At this time, the helicopter is experiencing a decelerated descent flight, with flight-path angle $\gamma = -10^\circ$. Inertial loads tangent to the trajectory, in combination with flight-path slope and pitch attitude rate of change, cause remarkable variation of hub force along the vehicle longitudinal axis, of in-plane hub moments, and hence of rotor α_{TPP} (conversely, C_T is barely affected by inertial loads). In this condition, approach A overestimates noise level, while approach B underestimates it. In terms of directivity, the two quasi-steady approaches present comparable results both on the hemisphere and on the ground, although approach B results seem to be slightly closer to approach C.

At the third point considered (see Figure 4), the helicopter is completing the pull-up maneuver, before entering a steady, level turn. Similarly to the first point, it is located at the end of a trajectory segment where remarkable inertial effects due to the trajectory curvature characterize the helicopter flight. In this case, they increase the rotor disk loading that is suitably captured by approach B. Flight parameters used to identify the noise source in

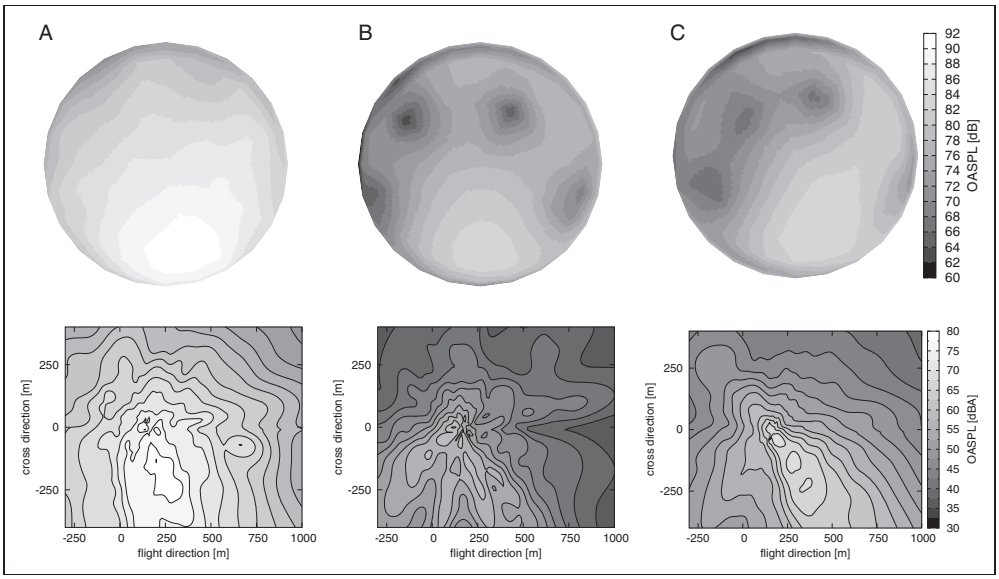

Figure 3. Noise hemispheres and noise footprints at $t = 6$ s.

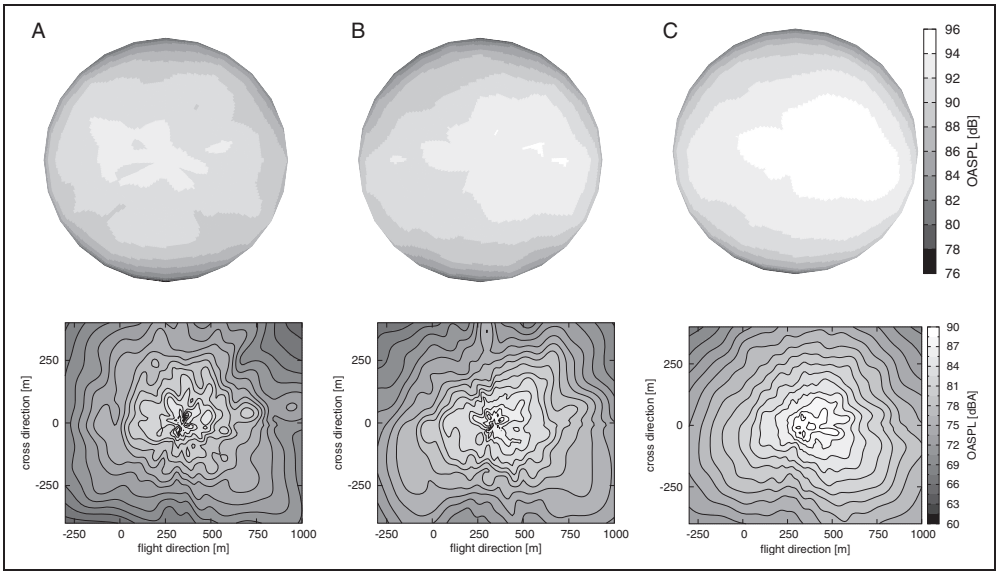

Figure 4. Noise hemispheres and noise footprints at $t = 14$ s.

approach A are such that this effect is not perceived, and hence the corresponding predicted acoustic disturbance is underestimated both on the hemisphere around the helicopter and on the ground. The spatial distribution of noise simulated by the three approaches is in good agreement and proves that the influence of BVI events on noise is of negligible entity.

Concluding remarks

Considering an unsteady helicopter maneuver, noise predictions determined by a fully unsteady numerical approach have been compared with those given by two quasi-steady noise simulation methods. The latter can be conveniently applied for low time-consuming predictions of the noise emitted by helicopters in unsteady flight as required, for instance, by optimal-noise trajectory search tools. A drawback can be the low level of accuracy in evaluating the radiated noise associated with the presence of unsteady effects during the maneuvering flight. Overall, the numerical investigation has demonstrated that the quasi-steady approach matching advance ratio, disk loading, and rotor attitude occurring during an unsteady maneuver (approach B) provides noise predictions of higher accuracy than those given by that matching only advance ratio and path-slope angle (approach A). This conclusion has been drawn especially for unsteady maneuver segments dominated by inertial effects influencing rotor disk loading. It has been noted that similar considerations may be drawn observing hemispheres connected to the helicopter or noise map evaluated on the ground with the inclusion of atmospheric attenuation effects. This suggests that, in absence of particular noise perturbation effects close to the ground, the near-field noise may provide a good measure of the quality of the predicted noise during unsteady maneuvers. For the flight conditions considered, the noise spatial distributions provided by the three approaches applied have been observed to be in good agreement.

Acknowledgements

Further, the authors wish to thank Mr. Alessio Castorrini for his help in obtaining flight dynamics simulations used in this work.

Declaration of conflicting interests

The author(s) declared no potential conflicts of interest with respect to the research, authorship, and/or publication of this article.

Funding

The author(s) disclosed receipt of the following financial support for the research, authorship, and/or publication of this article: The research leading to these results has received funding from Project MANOEUVRES, financed by European Community's Clean Sky Joint Undertaking Programme under Grant Agreement N. 620068.

References

1. Conner DA and Page JA. A tool for low noise procedures design and community noise impact assessment: the rotorcraft noise model (RNM). In: *Proceedings of Heli Japan 2002*, Tochigi, Japan, 2002.
2. Le Duc A, Spiegel P, Guntzer F, et al. Modelling of helicopter noise in arbitrary maneuver flight using aeroacoustic database. In: *Proceedings of ODAS 2008, 9th Onera-DLR aerospace symposium*, Châtillon, France, 2008.
3. Hartjes S, Buys Y, Visser HD, et al. Optimization of rotorcraft noise abatement trajectories. In: *Proceedings of internoise 2012/ASME NCAD meeting*, New York City, NY, USA, 2012, pp.1–19. American Society of Mechanical Engineers.

4. Morris RA, Venable KB and Lindsey J. Automated design of noise-minimal, safe rotorcraft trajectories. In: *Proceedings of the 68th annual forum of the American Helicopter Society*, vol. 1, Fort Worth, Texas, USA, 2012, pp.1–7. American Helicopter Society International.
5. Trainelli L, Rolando A, Zappa E, et al. MANOEUVRES – an effort towards quieter, reliable rotorcraft terminal procedures. In: *Proceedings of greener aviation: Clean sky breakthroughs and worldwide status*, Brussels, Belgium, 2014.
6. Brentner KS and Jones HE. Noise prediction for maneuvering rotorcraft. In: *Proceedings of the 6th AIAA/CEAS aeroacoustics conference*, Lahaina, Hawaii, USA, AIAA 2000-2031. America Institute of Aeronautics and Astronautics.
7. Janakiram RD and Khan H. Prediction and validation of helicopter descent flyover noise. In: *Proceedings of the 56th annual forum of the American Helicopter Society*, Virginia Beach, VA, USA, 2000. American Helicopter Society International.
8. Brentner KS, Perez G, Bres GA, et al. Toward a better understanding of maneuvering rotorcraft noise. In: *Proceedings of the 58th annual forum of the American Helicopter Society*, Montréal, Canada, 2002. American Helicopter Society International.
9. Bres GA, Brentner KS, Perez G, et al. Maneuvering rotorcraft noise prediction. *J Sound Vib* 2004; 275: 719–738.
10. Farassat F. Derivation of formulations 1 and 1A of Farassat. *NASA TM-2007-214853*. Hampton, VA, United States: NASA Langley Research Center, 2007.
11. Ffowcs Williams JE and Hawkings DL. Sound generated by turbulence and surface in arbitrary motion. *Philos Trans R Soc* 1996; A264: 321–342.
12. Hodges DH and Dowell EH. Nonlinear equation for the elastic bending and torsion of twisted nonuniform rotor blades. *NASA TN D-7818*. Moffett Field, CA, United States: NASA Ames Research Center, 1974.
13. Gennaretti M, Molica Colella M and Bernardini G. Prediction of tiltrotor vIbratory loads with inclusion of wing-proprotor aerodynamic interaction. *J Aircraft* 2010; 47: 71–79.
14. Gennaretti M and Bernardini G. Novel boundary integral formulation for blade-vortex interaction aerodynamics of helicopter rotors. *AIAA J* 2007; 45: 1169–1176.
15. Bernardini G, Serafini J, Molica Colella M, et al. Analysis of a structural-aerodynamic fully-coupled formulation for aeroelastic response of rotorcraft. *Aerosp Sci Technol* 2013; 29: 175–184.
16. Gennaretti M, Serafini J, Molica Colella M, et al. Simulation of helicopter noise in maneuvering flight. In: *Proceedings of 40th European Rotorcraft Forum*, Southampton, UK, 2014.
17. Gennaretti M, Serafini J, Bernardini G, et al. Numerical characterization of helicopter noise hemispheres. *Aerosp Sci Technol* 2016; 52: 18–28.
18. Hartjes S. *An optimal control approach to helicopter noise and emissions abatement terminal procedures*. PhD Thesis, Faculty of Aerospace Engineering, Delft University of Technology, Delft, The Netherlands, 2015.
19. International Civil Aviation Organization (ICAO). *International standards and recommended practices, environmental protection*. Annex 16, Volume I, Aircraft Noise, 5th ed., Montreal, Quebec, Canada: International Civil Aviation Organization, 2008.
20. Lamancusa JS and Daroux PA. Ray tracing in a moving medium with two-dimensional sound-speed variation and application to sound propagation over terrain discontinuities. *J Acoust Soc Am* 1993; 93: 1716–1726.
21. Delaney ME and Bazley EN. Acoustical properties of fibrous absorbent materials. *Appl Acoust* 1970; 3: 105–116.
22. Arntzen M, Rizzi SA, Visser HG, et al. A framework for simulation of aircraft flyover noise through a non-standard atmosphere. In: *Proceedings of the 18th AIAA/CEAS aeroacoustics conference*, Colorado Springs, CO, USA, 2012, AIAA 2012-2079. American Institute of Aeronautics and Astronautics.
23. Dang-Vu B, Masarati P, Quaranta G, et al. Generic helicopter database. Technical report deliverable No. D3.1, EU funded project ARISTOTEL (GA no. 266073), 2011.

24. Bernardini G, Serafini J, Ianniello S, et al. Assessment of computational models for the effect of aeroelasticity on BVI noise prediction. *Int J Aeroacoust* 2007; 6: 199–222.
25. Hodges DH and Ormiston RA. Stability of elastic bending and torsion of uniform cantilever rotor blades in hover with variable structural coupling. *NASA TN D-8192*. Moffett Field, CA, United States: NASA Ames Research Center, 1976.
26. Gennaretti M and Bernardini G. Aeroelastic response of helicopter rotors using a 3-D unsteady aerodynamic solver. *Aeronaut J* 2006; 110: 793–801.
27. Gennaretti M, Luceri L and Morino L. A unified boundary integral methodology for aerodynamics and aeroacoustics of rotors. *J Sound Vib* 1997; 200: 467–489.
28. Morino L and Bernardini G. Singularities in BIE's for the Laplace equation; Joukowski trailing-edge conjecture revisited. *J Eng Anal Bound Elem* 2001; 25: 805–818.
29. Ruijgrok GJJ. *Elements of aviation acoustics*. Delft: Delft University Press, 1993.
30. Chessell CI. Propagation of noise along a finite impedance boundary. *J Acoust Soc Am* 1977; 62: 825–834.

Appendix 1: Aeroelastic and aerodynamic main rotor modeling

The simulation of the acoustic disturbance generated by rotors is a multidisciplinary task: blade aeroelasticity and aerodynamics accurate modeling are required to yield the blade surface pressure distribution that, in turn, is the input to the aeroacoustic tool providing the near-field noise. When significant blade–wake interaction effects occur, blade–wake miss distance may play a crucial role, and hence the evaluation of blade deformation and wake shape is essential.[24]

Rotor aeroelastic modeling

Aeroelastic responses are obtained by combining a blade structural dynamics model with a three-dimensional, free-wake, potential-flow aerodynamics formulation.

Blade structural dynamics is described through a beam-like model. It derives from a nonlinear, bending-torsion formulation valid for slender, homogeneous, isotropic, nonuniform, twisted blades, undergoing moderate displacements.[12] The radial displacement is eliminated from the set of equations by solving it in terms of local tension, and thus the resulting structural operator consists of a set of coupled nonlinear differential equations governing the bending of the elastic axis and the blade torsion.[25]

The evaluation of the aerodynamic loads is obtained by a BEM for the solution of a boundary integral equation approach, suited for the analysis of potential flows around helicopter rotors in arbitrary flight condition[14] (see ''Rotor aerodynamic solver'' section).

Coupling blade structural dynamics with aerodynamic loads yields an aeroelastic integro-partial differential system of equations. These are spatially integrated through the Galerkin approach, with the description of elastic axis deformation and cross-section torsion as linear combinations of shape functions satisfying homogeneous boundary conditions. It yields a set of nonlinear, ordinary differential equations of the following type

$$\mathbf{M}(t)\,\ddot{\mathbf{q}} + \mathbf{C}(t)\,\dot{\mathbf{q}} + \mathbf{K}(t)\mathbf{q} = \mathbf{f}_{str}^{nl}(t, \mathbf{q}) + \mathbf{f}_{aer}(t, \mathbf{q}) \tag{4}$$

where $\mathbf{q}$ denotes the vector of the Lagrangian coordinates and $\mathbf{M}$, $\mathbf{C}$, and $\mathbf{K}$ are time-periodic, mass, damping, and stiffness structural matrices representing the linear structural terms.

Nonlinear structural contributions are collected in the forcing vector $\mathbf{f}_{str}^{nl}(t,\mathbf{q})$, whereas vector $\mathbf{f}_{aer}(t,\mathbf{q})$ collects the generalized aerodynamic forces.

The harmonic-balance approach is applied to determine the periodic aeroelastic response during steady flight.[15] It is a methodology suitable for the analysis of the asymptotic solution (as time goes to infinity) of differential equations forced by periodic terms and consists of: (i) express LHS and RHS of the aeroelastic system (equation (4)) in terms of their Fourier series; (ii) equate the resulting coefficients; (iii) solve the corresponding algebraic system in terms of the unknown Fourier coefficients of the Lagrangian coordinates of the problem. Specifically, expressing $\mathbf{q}$ and $\mathbf{f} = \mathbf{f}_{str}^{nl} + \mathbf{f}_{aer}$ in terms of the following Fourier series

$$\mathbf{q}(t) = \mathbf{q}_0 + \sum_{n=1}^{N} \left[\mathbf{q}_n^c \cos(\Omega_n t) + \mathbf{q}_n^s \sin(\Omega_n t)\right]$$

$$\mathbf{f}(t) = \mathbf{f}_0 + \sum_{n=1}^{N} \left[\mathbf{f}_n^c \cos(\Omega_n t) + \mathbf{f}_n^s \sin(\Omega_n t)\right]$$

(where $\mathbf{q}_n^c, \mathbf{q}_n^s, \mathbf{f}_n^c$, and $\mathbf{f}_n^s$ denote cosine and sine components of the nth harmonic of $\mathbf{q}$ and $\mathbf{f}$, whereas $\Omega_n = n\Omega$, with Ω representing the fundamental frequency, i.e. the rotor angular velocity) and then combining with equation (4) yields the following representation of the aeroelastic system harmonic components

$$\left[\widehat{\mathbf{M}} + \widehat{\mathbf{C}} + \widehat{\mathbf{K}}\right]\widehat{\mathbf{q}} = \widehat{\mathbf{f}} \tag{5}$$

where $\widehat{\mathbf{q}}^T = \left\{\mathbf{q}_0\ \mathbf{q}_1^c\ \mathbf{q}_1^s\ \mathbf{q}_2^c\ \mathbf{q}_2^s\ \cdots\right\}$ and $\widehat{\mathbf{f}}^T = \left\{\mathbf{f}_0\ \mathbf{f}_1^c\ \mathbf{f}_1^s\ \mathbf{f}_2^c\ \mathbf{f}_2^s\ \cdots\right\}$. Matrices $\widehat{\mathbf{M}}, \widehat{\mathbf{C}}$, and $\widehat{\mathbf{K}}$ in equation (5) come out from equation (4) by combining the harmonics of the $\mathbf{q}, \dot{\mathbf{q}}$, and $\ddot{\mathbf{q}}$ terms with the harmonics of the matrices $\mathbf{M}, \mathbf{C}$, and $\mathbf{K}$. In particular, if $\mathbf{M}, \mathbf{C}$, and $\mathbf{K}$ were constant matrices, in equation (5) one would have block diagonal matrices and each harmonic of $\mathbf{q}$ would depend only on the same harmonic of $\mathbf{f}$ (the $\mathbf{q}$-harmonics equations would be uncoupled). Instead, in the problem under examination the structural matrices are periodic and hence, once expressed in terms of the Fourier series and combined with the harmonics of $\mathbf{q}, \dot{\mathbf{q}}$, and $\ddot{\mathbf{q}}$, they yield fully populated $\widehat{\mathbf{M}}, \widehat{\mathbf{C}}$, and $\widehat{\mathbf{K}}$ matrices, thus coupling the algebraic equations for the unknown harmonics in $\widehat{\mathbf{q}}$ (see, for instance Gennaretti and Bernardini[26]).

Because of the presence of nonlinear structural terms and of aerodynamic contributions in $\widehat{\mathbf{f}}$, equation (5) has to be solved using an iterative procedure. To this aim, the Newton–Raphson method with a simplified Jacobian matrix is applied. Specifically, the harmonic aeroelastic solution is obtained from convergence of the following iterative procedure (with n indicating the iteration step number)

$$\widehat{\mathbf{q}}_n = \left[\widehat{\mathbf{M}} + \widehat{\mathbf{C}} + \widehat{\mathbf{K}} - \widehat{\mathbf{J}}_{aer}\right]^{-1}[\widehat{\mathbf{f}}_{n-1} - \widehat{\mathbf{J}}_{aer}\widehat{\mathbf{q}}_{n-1}] \tag{6}$$

where $\widehat{\mathbf{J}}_{aer}$ is the aerodynamic Jacobian evaluated at $\widehat{\mathbf{q}} = \mathbf{0}$, while $\widehat{\mathbf{f}}_{n-1}$ denotes the nonlinear structural terms and aerodynamic loads evaluated at $\widehat{\mathbf{q}} = \widehat{\mathbf{q}}_{n-1}$ (i.e. through the Lagrangian coordinates given by the previous iteration step). Under this assumption, the aerodynamic portion of the forcing term is equivalent to $\widehat{\mathbf{f}}_{aer}^0 + \widehat{\mathbf{f}}_{aer}^{nl}$, with $\widehat{\mathbf{f}}_{aer}^0$ denoting the aerodynamic load portion that is not influenced by the structural deformation. The introduced approximation of the Jacobian is convenient in that it implies that the matrix inversion required in equation (6) has to be evaluated only one time. If convergence problems arise (because of

large differences between the local aerodynamic gradient and $\widehat{\mathbf{J}}_{aer}$), the aerodynamic Jacobian and the inversion of the global Jacobian matrix have to be reevaluated during the iteration process.

Note that nonperiodic aeroelastic responses during unsteady helicopter maneuvers are evaluated through a time-marching solution algorithm based on the Newmark-β integration scheme.

Rotor aerodynamic solver

Considering incompressible, potential flows such that $\mathbf{v} = \nabla\varphi$, the rotor aerodynamics formulation applied assumes the potential field, φ, to be given by the superposition of an incident field, φ_I, and a scattered field, φ_S (i.e. $\varphi = \varphi_I + \varphi_S$). The scattered potential is determined by sources and doublets distributions over the surfaces of the blades, S_B, and by doublets distributed over the wake portion that is very close to the trailing edge from which emanated (near wake, S_W^N). The incident potential field is associated to doublets distributed over the complementary wake region that compose the far wake S_W^F.[14] The wake surface partition is such that the far wake is the only wake portion that may come in contact with blades and generate BVI effects. The incident potential is discontinuous across S_W^F, whereas the scattered potential is discontinuous across S_W^N and is represented by[14]

$$\varphi_S(\mathbf{x}, t) = \int_{S_B} \left[G(v_n - u_n) - \varphi_S \frac{\partial G}{\partial n} \right] \mathrm{d}S(\mathbf{y}) - \int_{S_W^N} \Delta\varphi_S \frac{\partial G}{\partial n} \mathrm{d}S(\mathbf{y}) \tag{7}$$

where $G = -1/4\pi r$ is the unit-source solution of the three-dimensional Laplace equation, with $r = ||\mathbf{y} - \mathbf{x}||$, while $\Delta\varphi_S$ is the potential jump across the wake surface, known from past history of potential discontinuity at the blade trailing edge through the Kutta–Joukowski condition.[27,28] In addition, $v_n = \mathbf{v}_B \cdot \mathbf{n}$, with $\mathbf{v}_B$ representing the blade velocity and $\mathbf{n}$ its outward unit normal, whereas $u_n = \mathbf{u}_I \cdot \mathbf{n}$, with $\mathbf{u}_I$ denoting the velocity induced by the far wake, which is given by

$$\mathbf{u}_I(\mathbf{x}, t) = \nabla\varphi_I(\mathbf{x}, t) = -\nabla \int_{S_W^F} \Delta\varphi_S\left(\mathbf{y}_W^{TE}, t - \vartheta\right) \frac{\partial G}{\partial n} \mathrm{d}S(\mathbf{y}) \tag{8}$$

Considering the far wake discretized into M panels, assuming the potential jump constant over each panel, and recalling the equivalence between surface distribution of doublets and vortices, the incident velocity field is evaluated through the following application of the Biot–Savart law to the vortices having the shape of the panels contour

$$\mathbf{u}_I(\mathbf{x}, t) \approx -\sum_{k=1}^{N} \Delta\varphi_S\left(\mathbf{y}_{W_k}^{TE}, t - \vartheta_k\right) \int_{C_k} \nabla_{\mathbf{x}} G \times \mathrm{d}\mathbf{y} \tag{9}$$

where C_k denotes the contour line of the kth far wake panel, $\mathbf{y}_{W_k}^{TE}$ is the trailing edge position where the wake material point currently in $\mathbf{y}_{W_k}$ emanated at time $t - \vartheta_k$, and $\nabla_{\mathbf{x}}$ denotes gradient operator with respect to the variable $\mathbf{x}$.

In order to assure a regular distribution of the induced velocity within the vortex core, and thus a stable and regular solution even in blade–vortex impact conditions, a Rankine finite-thickness vortex model is introduced in the Biot–Savart law.[14] The wake-induced velocity field is applied to evaluate the term u_n in Equation (7) as well as the velocity field from which the wake shape evolution is determined in a free-wake analysis. Note that, for an

accurate prediction of BVI phenomena, the accurate evaluation of the wake distorted shape is essential in that a crucial role is played by the relative position between body and wake.

In this formulation, the incident potential affects the scattered potential through the induced velocity, while the scattered potential affects the incident potential by its trailing-edge discontinuity that is convected along the wake and yields the intensity of far-wake vortices.[14] Once the potential field is known, the Bernoulli theorem yields the pressure distribution to be provided to aeroelastic and aeroacoustic solvers.[15]

Appendix 2: Atmospheric noise propagation algorithm

To assess the noise impact on the ground, the source noise levels available from the hemispherical database need to be propagated to the ground. In this study, spreading loss, ground effect, and atmospheric absorption are accounted for, all taking into account propagation through a refracting medium. The first step in determining the total propagation loss is to determine the ray path, i.e. the path the sound waves follow from source to receiver. The ray path is constructed using a geometrical approach to ray tracing. The atmosphere is divided in a number of layers, and in each of the layers a constant speed-of-sound gradient is assumed. Consequently, refraction occurs within each layer. The radius of curvature of the ray path is defined as

$$R_i = \frac{-c_i}{g_i \cos\theta_{0,i}} \tag{10}$$

where c_i is the speed of sound at the top of the layer, and g_i the linearized gradient in the layer. The center of curvature is then defined by

$$x_{c,i} = x_{0,i} + R_i \sin\theta_{0,i} \tag{11}$$

$$z_{c,i} = z_{0,i} + R_i \cos\theta_{0,i} \tag{12}$$

This allows to calculate the final angle of incidence $\theta_{f,i}$, final distance $x_{f,i}$, and the arc segment length s_i

$$\theta_{f,i} = \cos^{-1}\left(\frac{z_c - z_{f,i}}{R_i}\right) \tag{13}$$

$$x_{f,i} = x_c - R_i \sin\theta_{f,i} \tag{14}$$

$$s_i = ||R_i(\theta_{f,i} - \theta_{0,i})|| \tag{15}$$

Repeating this process for each of the layers then yields the complete ray path. The next step is to determine the propagation loss along each ray path. In a refracting atmosphere, ray paths can converge or diverge, and as such a correction needs to be applied to the spherical spreading loss. This correction is based on the distance between two ray paths launched at a small incremental angle, $\Delta\theta_0$. It can be shown[20] that for relatively low wind speeds, the total spreading loss can be defined as

$$\Delta SPL_S = -10\log_{10}\left(\frac{A_r}{A_u}\right) + 20\log_{10}\left(\frac{s_0}{s_r}\right) \tag{16}$$

where A_r and A_u are the distances between the two ray paths in a refracting and nonrefracting medium, respectively, and the second term represents standard spherical spreading from the source at distance s_0 to a distance s_r along the ray path. To correct for absorption along

the ray path, the method defined by the ICAO[19] has been applied. This method defines the atmospheric attenuation coefficient, α, as

$$\alpha = 10^{\left[2.05\log_{10}\left(\frac{f_0}{1000}\right)+1.1394\cdot10^{-3}T-1.916984\right]} + \eta(\delta)\cdot 10^{\left[\log_{10}(f_0)+8.42994\cdot10^{-3}T-2.755624\right]} \tag{17}$$

where δ is defined as

$$\delta = \sqrt{\frac{1010}{f_0}}10^{\left[\log_{10}H-1.328924+3.179768\cdot10^{-2}T\right]} \times 10^{\left[-2.173716\cdot10^{-4}T^2+1.7496\cdot10^{-6}T^3\right]} \tag{18}$$

and η is derived through a table lookup. For relatively low frequencies up to 4000 Hz $f_0 = f$ applies. The total absorption loss can then be defined as

$$\Delta SPL_A = \frac{\alpha s}{100} \tag{19}$$

The final correction applied to the source noise levels is the ground effect. When two sound rays—a direct ray and a ray reflected off the ground surface—reach an observer, the phase shift between the rays results in either an increase or decrease of the total sound pressure. It can be shown[29,30] that depending on the difference in the ray path length $s_2 - s_1$ between a direct and a reflected ray, the ground effect can be defined as

$$\Delta SPL_G = 20\log_{10}\left|1 + \frac{s_1}{s_2}Qe^{ik(s_2-s_1)}\right| \tag{20}$$

where k is the wave number and Q is the reflection factor. The latter is a property of the ground surface and depends on the final angle of incidence θ_f determined from the ray path construction and the normal surface impedance Z_n of the ground surface[30]

$$Q = \frac{\frac{Z_n}{\rho_0 c_0}\sin\theta_f - 1}{\frac{Z_n}{\rho_0 c_0}\sin\theta_f + 1} \tag{21}$$

The specific normal acoustic impedance Z_n can be expressed as follows[21]

$$\frac{Z_n}{\rho_0 c_0} = 1 + 0.0511\left(\frac{f}{\sigma}\right)^{-0.75} + i0.0768\left(\frac{f}{\sigma}\right)^{-0.73} \tag{22}$$

and depends on the frequency and the effective flow resistivity σ of the ground surface. The final sound level reaching the observer is then found by adding each of the propagation losses to the source noise levels found from the hemispherical database.